Static response of a jellium surface: The image potential and indirect interaction between two charges

A. G. Eguiluz, D. A. Campbell, A. A. Maradudin, and R. F. Wallis
Department of Physics, University of California, Irvine, California 92717
(Received 7 March 1984; revised manuscript received 26 July 1984)

We present detailed numerical results for the energy of interaction between a static charge and a jellium surface and for the total energy of interaction between two static charges placed in the surface region. In the latter case we obtain some novel results showing the disappearance of the bulk oscillatory behavior in the total interaction energy as the two charges are brought from inside the metal surface and placed outside the jellium edge. Both response calculations are performed by first computing the static electron-density response function in the random-phase approximation. The response function for noninteracting electrons (the irreducible part of the linear response) is obtained on the basis of a computational method that renders the eigenfunctions $\psi_\nu(\vec{x})$ of the Kohn-Sham equations of a jellium slab in semianalytical form. This method consists of expanding the dependence of $\psi_\nu(\vec{x})$ on the coordinate normal to the jellium surfaces in a sine series and solving a nonlinear matrix version of the Kohn-Sham self-consistent problem.

I. INTRODUCTION

This paper is part of an ongoing effort dedicated to the study of the response of metal surfaces to probes such as external charges placed near the surface, or the phonon field associated with the vibrations of the outer atomic layers. In such problems a central role is played by the static density response function $\chi(\vec{x},\vec{x}')$ defined by the equation

$$n_{\rm ind}(\vec{x})=\int d^3x'\chi(\vec{x},\vec{x}')U_{\rm ext}(\vec{x}')\,, \tag{1.1}$$

where $n_{\rm ind}(\vec{x})$ is the electron number density induced by an external longitudinal field $U_{\rm ext}(\vec{x})$.

A basic ingredient in the integral equation[1] satisfied by $\chi(\vec{x},\vec{x}')$ is the response function for noninteracting electrons confined by an effective potential $V_{\rm eff}(\vec{x})$, $\chi^{(0)}(\vec{x},\vec{x}')$, given at the absolute zero of temperature by

$$\chi^{(0)}(\vec{x},\vec{x}')=\sum_{\nu,\nu'}\left[\frac{f_\nu-f_{\nu'}}{\epsilon_\nu-\epsilon_{\nu'}}\right]\psi_\nu(\vec{x})\psi_{\nu'}^*(\vec{x})\times\psi_{\nu'}(\vec{x}')\psi_\nu^*(\vec{x}')\,, \tag{1.2}$$

In this expression $f_\nu=2\Theta(E_F-\epsilon_\nu)$, where E_F is the Fermi energy and $\Theta(x)$ is the unit step function. The wave functions $\psi_\nu(\vec{x})$ and the effective potential $V_{\rm eff}(\vec{x})$ are related through the self-consistent Kohn-Sham equation[2]

$$\left[-\frac{\hbar^2}{2m}\nabla^2+V_{\rm eff}(\vec{x})\right]\psi_\nu(\vec{x})=\epsilon_\nu\psi_\nu(\vec{x})\,, \tag{1.3}$$

with

$$V_{\rm eff}(\vec{x})=v(\vec{x})+e^2\int d^3x'\frac{n(\vec{x}')}{|\vec{x}-\vec{x}'|}+V_{\rm xc}(\vec{x})\,. \tag{1.4}$$

In Eq. (1.4) $v(\vec{x})$ is the potential for the interaction with the ionic background, $n(\vec{x})$ is the electron number density, given at the absolute zero of temperature by

$$n(\vec{x})=\sum_\nu f_\nu|\psi_\nu(\vec{x})|^2\,, \tag{1.5}$$

and the exchange and correlation potential $V_{\rm xc}(\vec{x})$ is defined by the equation

$$V_{\rm xc}(\vec{x})=\frac{\delta E_{\rm xc}[n]}{\delta n(\vec{x})}\,, \tag{1.6}$$

where $E_{\rm xc}[n]$ is the exchange and correlation energy functional [it embodies all the many-body effects in Eq. (1.3)].

The point of view adopted in the present work is that the complexity of earlier calculations of the surface response[1,3,4] stems to a large extent from the fact that the wave functions $\psi_\nu(\vec{x})$ have traditionally been obtained entirely numerically. It seems clear that if we had a representation for these wave functions in a simple basis set, the computation of $\chi^{(0)}(\vec{x},\vec{x}')$ and thus of $\chi(\vec{x},\vec{x}')$, and ultimately of any surface response properties obtained from the latter would be greatly facilitated.

In this paper we present a computational scheme that, for the case of a metal film and in the jellium model for the periodic background, renders the electron wave functions $\psi_\nu(\vec{x})$ in semianalytical form. Our method consists of expanding the dependence of $\psi_\nu(\vec{x})$ on the coordinate normal to the jellium surfaces in a sine series. The coefficients of such an expansion are obtained by solving a nonlinear matrix version of the above self-consistent problem. (The local-density approximation[2] for the functional $E_{\rm xc}[n]$ is used.) The details of our procedure are given in Sec. II.

Having obtained a simple representation for the wave functions $\psi_\nu(\vec{x})$, in Sec. III we illustrate the simplicity of the calculation of the surface response afforded by our

method by presenting detailed numerical results for two physically interesting surface response problems. The first is the determination of the energy of interaction between a static charge and a jellium surface. In particular, we obtain the position of the effective image plane,[3,4] which is shown to depend sensitively on the details of the electron-density profile at the surface. The second is the calculation of the total energy of interaction between two static charges placed in the vicinity of the surface. This energy includes the indirect interaction between the charges mediated by the polarization of the surface.[5] We show that for values of the lateral separation between the charges representative of adatom-adatom distances in chemisorption, the total interaction energy decays *monotonically* with distance when the charges are at the surface (jellium edge) or outside it. As the charges are moved into the metal interior, Friedel oscillations in the total interaction energy rapidly build up. The key ingredient in both calculations is the density response function $\chi(\vec{x},\vec{x}')$, which in this work is obtained in the random-phase approximation (RPA). The application of our formalism to the study of lattice dynamical properties of a metal surface will be the subject of a forthcoming publication.

We close this introduction by noting that although the formalism developed in this paper makes essential use of the assumption of a finite (in practice, rather small) film thickness, it nonetheless proves useful for the study of the response of a *semi-infinite* medium. The reason for this is that the static electron screening length is, at metallic densities, of the order of a few angstroms.

II. THE EIGENVALUE PROBLEM FOR THE GROUND STATE

A. Statement of the problem

In this section we are concerned with solving Eq. (1.3) for a metal slab with the use of the jellium model for the periodic background. The physical situation we consider is depicted in Fig. 1. The two parallel faces of a jellium slab of thickness a and constant charge density $\rho_+ = e\bar{n}_+$ are assumed to be normal to the z axis. (We denote by e the magnitude of the electron charge.) Periodic boundary conditions are imposed on the slab in the x and y directions. The normalization area in the x-y plane is A. Now the electrons, whose total number is $N = aA\bar{n}_+$, distribute themselves in such a way that the total energy of the system is minimized. From the Lang-Kohn solution[6] of the self-consistent ground-state problem for the semi-infinite medium we know that outside the jellium edge the electron-density profile $n_0(z)$ decays rapidly from its bulk value $\bar{n}_+$. [It decays by several orders of magnitude for a distance from the jellium $z \sim \lambda_F = 2\pi/k_F$, where k_F is the Fermi wave vector, of 0 (1 Å^{-1}).] It is then convenient to render the electronic system strictly finite in the z direction by assuming that $N_0(z)$ actually vanishes at a finite distance (denoted by z_0) from the jellium edge. From the point of view of the Schrödinger equation (1.3) this assumption implies the introduction of infinite potential walls at a distance z_0 from each jellium edge.[7,8] The expectation is that for sufficiently large values of z_0 any physical observables calculated on the basis of our model are independent of the precise choice of z_0.

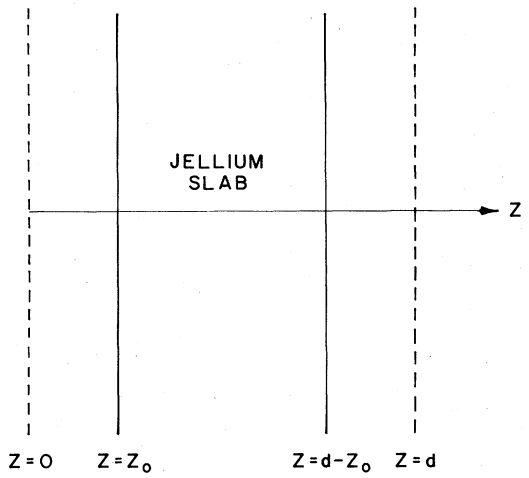

FIG. 1. Physical system considered in the present work.

In the jellium model, the wave functions $\psi_\nu(\vec{x})$ can be written in the form

$$\psi_\nu(\vec{x}) = \frac{1}{A^{1/2}} e^{i\vec{k}_{||}\cdot\vec{x}_{||}} \phi_l(z) , \tag{2.1}$$

where $\vec{x}_{||}$ and $\vec{k}_{||}$ are, respectively, position and wave vectors in the x-y plane. Making use of Eq. (2.1) in Eq. (1.5) we have that

$$n(\vec{x}) \equiv n_0(z) = \frac{m}{\pi\hbar^2} \sum_l \Theta(E_F - \epsilon_l)(E_F - E_l)\phi_l^2(z) , \tag{2.2}$$

where the Fermi energy E_F is determined by the condition

$$N = \frac{mA}{\pi\hbar^2} \sum_l \Theta(E_F - E_l)(E_F - \epsilon_l) . \tag{2.3}$$

Equation (2.2) shows explicitly that the ground-state electron-density profile $n_0(z)$ is a function of the z coordinate only. Equation (1.3) reduces then to a one-dimensional Schrödinger equation for the wave functions $\phi_l(z)$, namely

$$\left[-\frac{\hbar^2}{2m}\frac{d^2}{dz^2} + V_{\text{eff}}(z) \right] \phi_l(z) = \epsilon_l \phi_l(z) , \tag{2.4}$$

where the energy eigenvalues ϵ_l are defined by

$$\epsilon_\nu = \epsilon_{l,\vec{k}_{||}} = \frac{\hbar^2 k_{||}^2}{2m} + \epsilon_l, \quad l = 1,2,3,\ldots . \tag{2.5}$$

The effective potential $V_{\text{eff}}(z)$ is given by the equation

$$V_{\text{eff}}(z) = V_\infty(z) + V_H(z) + V_{\text{xc}}(z) , \tag{2.6}$$

where $V_\infty(z)$ is the potential for the above-mentioned infinite well, and the total electrostatic potential $V_H(z)$ is given by the equation

$$V_H(z) = -2\pi e^2 \int_0^d dz' [n_0(z') - n_+(z')] \, | z - z' | , \tag{2.7}$$

with

$$n_+(z)=\begin{cases}\bar{n}_+, & z_0<z<d-z_0\\ 0, & \text{otherwise}.\end{cases} \tag{2.8}$$

In this work we adopt the local-density approximation[2] for $V_{xc}(z)$. For the exchange potential we use the local Slater approximation[2] reduced by a factor of $\frac{2}{3}$, and for the correlation potential we use the local Wigner interpolation approximation.[2]

Equations (2.2)—(2.8) define the self-consistent problem to be solved, a path well trodden by density functional practitioners. As indicated in the Introduction, our purpose in this work is to present an alternative solution to the conventional numerical integration of Eq. (2.4), a solution that renders the wave functions $\phi_l(z)$ in semianalytical form.

B. Matrix form of the eigenvalue problem and numerical solution

In view of the limited range of variation of the variable z, namely $0<z<d$, and the infinite potential barrier at each end point of this interval, we choose to expand the wave functions $\phi_l(z)$ in a Fourier sine series,

$$\phi_l(z)=\left[\frac{2}{d}\right]^{1/2}\sum_{s=1}^{\infty}a_s^{(l)}\sin\left[\frac{s\pi}{d}z\right]. \tag{2.9}$$

Substituting Eq. (2.9) in (2.4), multiplying the latter equation on the left by $(2/d)^{1/2}\sin(p\pi z/d)$, and integrating over z, we obtain the following matrix version of Eq. (2.4):

$$\sum_{p'=1}^{\infty}M_{pp'}a_{p'}^{(l)}=\epsilon_l a_p^{(l)},\quad p=1,2,3,\ldots. \tag{2.10}$$

The matrix $M_{pp'}$ is defined in Appendix A.

Equation (2.10) has to be solved self-consistently because the eigenvector $\{a_s^{(l)}\}$ being sought appears in the elements of the matrix $M_{pp'}$. As is well known, the self-consistent solution by iteration is plagued by instabilities. We have followed a standard "attenuated mixing" scheme, more sophisticated versions of which have been given recently by Kerker[9] and by Ho *et al.*[10] In general, the thicker the film, the smaller the mixing parameter. For example, in the case of aluminum, for a five-layer film we added 20% of the "new" eigenvector to 80% of the "old" eigenvector (or a mixing parameter of 20%) to give the next eigenvector in the iteration scheme. For a 20-layer film we used a mixing parameter of 1%. In the latter case, the number of iterations required is on the order of 100.

Another aid to speeding convergence is a "stretching" procedure similar to the one used, for example, by Feibelman *et al.*[11] In the case of a high-density metal such as aluminum, it is found that for a film thickness as small as three atomic layers the electron-density profile is, in the neighborhood of each jellium edge, remarkably close to that for the semi-infinite medium (or the Lang-Kohn profile). Thus one can "prepare" an initial guess for the electron-density profile $n_0(z)$ for a thicker film (for example, 15 layers thick) by adding to the profile obtained for a thinner film (for example, 5 layers thick) a flat central piece with the bulk value of the electron density. With this "stretched" profile as our initial guess, we evaluate the integrals in Eqs. (A2) and (A3) numerically, and the matrix $M_{pp'}$ so generated is diagonalized for the first time.

Two significant parameters in our model are the distance z_0 from the jellium edge to the point where $n_0(z)$ is taken to vanish, and the number of sines ($\equiv s_{\max}$) kept in the expansion (2.9) of the electron wave functions. We find that in order to reproduce the Lang-Kohn density profile to better than 1% accuracy $z_0\gtrsim 1.5a_0$ is needed, where a_0 is the lattice constant of the metal. The value of $s_{\max}$ depends on the film thickness and on z_0 (the bigger z_0, the larger $s_{\max}$). It is to be noted that the rank of the matrix $M_{pp'}$ equals $s_{\max}$. Thus $s_{\max}$ has to be at least equal to the number of occupied electron states ($\equiv l_M$). In practice $s_{\max}$ is substantially greater than l_M. This automatically provides us with the wave functions for a number of the unoccupied states (which are used in the computation of the electron-gas response).

In Figs. 2—4 we illustrate the dependence of our numerical results for $n_0(z)$ on the parameters z_0 and $s_{\max}$ and on the film thickness. These results supersede those given for sodium in a preliminary report,[8] in which full convergence was not achieved. In Fig. 2 we show results for $n_0(z)$ for a five-layer sodium film, obtained for $s_{\max}=10$, 20, and 30, respectively, with $z_0=1.5a_0$. Note that the profiles obtained for $s_{\max}=20$ and 30 are indistinguishable on the scale of the figure. We also show the profile obtained for a nine-layer film. Note that the converged profiles for five and nine layers differ mainly in the Friedel-oscillation region. Further increase in the film thickness (beyond nine layers) leaves $n_0(z)$ unchanged on the scale of the figure. In Figs. 3 and 4 we show the electron-density profile $n_0(z)$ for nine-layer aluminum and

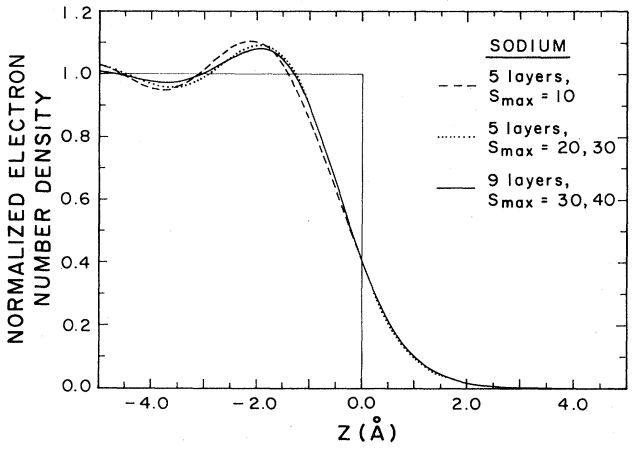

FIG. 2. Dependence of the electron-density profile $n_0(z)/\bar{n}_+$ for sodium on the number of sines ($\equiv s_{\max}$) used in Eq. (2.9) and on the film thickness. The profile obtained for a nine-layer film remains unchanged for thicker films. In this figure we have used $z_0=1.5a_0$ (see text).

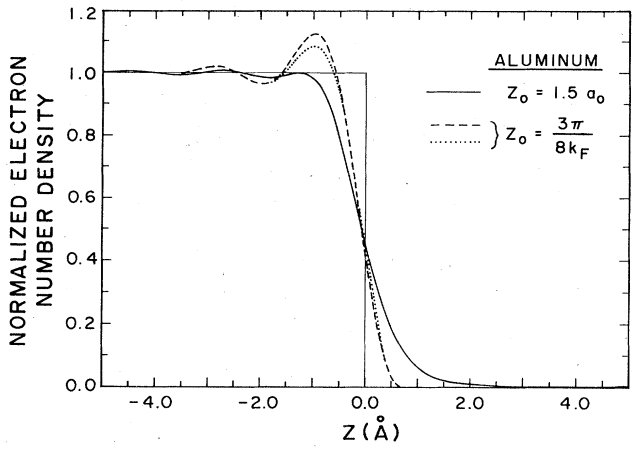

FIG. 3. Dependence of the electron-density profile $n_0(z)/\bar{n}_+$ for aluminum on the value of z_0 giving the position of the effective infinite potential walls. For $z_0=1.5a_0(=6.075$ Å) the profile agrees with the Lang-Kohn profile throughout the surface region to better than 1%. For $z_0=3\pi/8k_F(=0.673$ Å), we show both the IBM profile (dotted line) and the profile obtained keeping the full Hamiltonian matrix $M_{pp'}$ in Eq. (2.10) (dashed line).

sodium films obtained for $z_0=1.5a_0$, and $s_{\max}=40$ and 30, respectively. In each case the profile is identical, on the scale of the figure, to the Lang-Kohn profile.[6] In both Figs. 3 and 4 we also show the profiles obtained for a smaller value of z_0. For illustrative purposes we took $z_0=3\pi/8k_F$, which is the value that obtains (for a thick film) in the infinite-barrier model (IBM).[12,13] In the IBM there are no electron-electron interactions in the ground state and the wave functions $\phi_l(z)$ are given by Eq. (2.9) with $a_s^{(l)}=\delta_{sl}$. For this value of z_0 we show the profile obtained by the self-consistent solution of Eq. (2.10) and also the IBM profile.[12] Note that although we find that for this small value of z_0 the coefficients $a_s^{(l)}$ are nearly equal to δ_{ls} [that is, the wave functions $\phi_l(z)$ are nearly sines], the corresponding profiles differ appreciably.

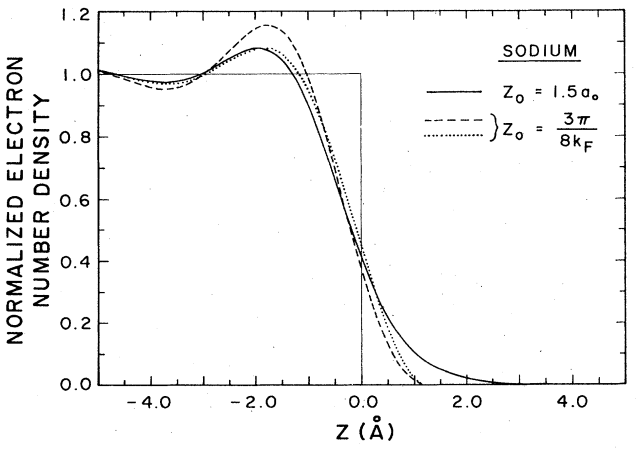

FIG. 4. Same as Fig. 3, but for a sodium film. In this case $1.5a_0=6.337$ Å and $3\pi/8k_F=1.278$ Å.

III. APPLICATION TO THE STUDY OF THE SURFACE RESPONSE OF THE ELECTRON GAS

In this section we illustrate the application of the method developed in Sec. II to the study of linear-response properties of the electron gas at the surface of a nearly-free-electron metal.

In the jellium model for the periodic background the relevant density response function is the two-dimensional Fourier transform $\chi(q_{||}\,|\,z,z')$ of the full response function $\chi(\vec{x},\vec{x}\,')$ defined in Eq. (1.1). We have that

$$\chi(\vec{x},\vec{x}\,')=\int \frac{d^2q_{||}}{(2\pi)^2}e^{i\vec{q}_{||}\cdot(\vec{x}_{||}-\vec{x}\,'_{||})}\chi(q_{||}\,|\,z,z')\ . \tag{3.1}$$

In this work we evaluate χ within the random-phase approximation (RPA). In the RPA, $\chi(q_{||}\,|\,z,z')$ obeys the integral equation[14,15]

$$\chi(q_{||}\,|\,z,z')=\chi^{(0)}(q_{||}\,|\,z,z') + \int_0^d dz_1 \int_0^d dz_2\chi^{(0)}(q_{||}\,|\,z,z_1) \times v(q_{||}\,|\,z_1,z_2)\chi(q_{||}\,|\,z_2,z')\ , \tag{3.2}$$

where

$$v(q_{||}\,|\,z_1,z_2)=\frac{2\pi e^2}{q_{||}}e^{-q_{||}|z_1-z_2|} \tag{3.3}$$

is the two-dimensional Fourier transform of the Coulomb potential energy and $\chi^{(0)}(q_{||}\,|\,z,z')$ is the two-dimensional Fourier transform of the density response function for noninteracting electrons defined in Eq. (1.2). An explicit result for $\chi^{(0)}(q_{||}\,|\,z,z')$ can be found in Ref. 15.

The solution of Eq. (3.2) has recently been given by Eguiluz,[15] and we refer the reader to his work for a detailed discussion. Here we shall simply note that we introduce a double-cosine Fourier representation for the response function[14–16] defined by the equation

$$\chi(q_{||}\,|\,z,z')=\sum_{m=0}^{\infty}\sum_{n=0}^{\infty}\chi_{mn}(q_{||}) \times\cos\left[\frac{m\pi}{d}z\right]\cos\left[\frac{n\pi}{d}z'\right]\ , \tag{3.4}$$

with similar expansions for $\chi^{(0)}(q_{||}\,|\,z,z')$ and $v(q_{||}\,|\,z_1,z_2)$, and transform Eq. (3.2) into a matrix equation for the coefficients $\chi_{mn}(q_{||})$ that is solved numerically. The key ingredient of that matrix equation is the matrix of the coefficients $\chi^{(0)}_{mn}(q_{||})$ of $\chi^{(0)}(q_{||}\,|\,z,z')$, which is directly obtainable by algebraic means from the wave functions $\phi_l(z)$ through their coefficients $a_s^{(l)}$ defined in Eq. (2.9). This is the reason for the simplicity of our response calculation.

From a knowledge of the coefficients $\chi_{mn}(q_{||})$ of the density response function we can proceed to study the interaction of the surface with various longitudinal probes. In this paper we consider two simple examples.

A. Energy of interaction between a static charge and a jellium surface

In the present case the external potential $U_{\rm ext}(\vec{x};\vec{R}_1)$ [cf. Eq. (1.1)] is

$$U_{\rm ext}(\vec{x};\vec{R}_1)=-\frac{eQ_1}{|\vec{x}-\vec{R}_1|}\ , \tag{3.5}$$

where $\vec{R}_1$ denotes the (fixed) position of the external particle and Q_1 its charge. From Eqs. (3.5), (1.1), and (3.1) and the solution of Eq. (3.2), we obtain the induced charge density $-en_{\rm ind}(\vec{x})$, and from it the screening (induced) field, given by the equation

$$\vec{E}_{\rm ind}(\vec{x})=e\vec{\nabla}\int d^3x'\frac{n_{\rm ind}(\vec{x}')}{|\vec{x}-\vec{x}'|}\ . \tag{3.6}$$

For $\vec{x}=\vec{R}_1$ Eq. (3.6) gives the screening field at the position of the external charge. The work required to bring the charge from infinity to the point $\vec{R}_1=(0,0,z_1)$ against this field is the so-called image potential $U_{\rm im}(z_1)$. We obtain the result that

$$U_{\rm im}(z_1)=\int_0^\infty dq_{||}\sum_{mn}A_{mn}(q_{||}\,|\,z_1)\chi_{mn}(q_{||})\ . \tag{3.7}$$

The matrix $A_{mn}(q_{||}\,|\,z_1)$ is given in Appendix B. Equation (3.7) generalizes the classical image potential

$$U_{\rm cl}(z_1)=-\frac{e^2}{4(z_1-z_{\rm im})}\ , \tag{3.8}$$

where $z_{\rm im}$ is the position of the effective image plane.[3,4,17]

The result given by Eq. (3.7) reduces the evaluation of the image potential to carrying out matrix algebra on the computer [on the basis of the knowledge of the matrix $\chi_{mn}(q_{||})$] followed by an integration over all wave-vector transfers. It is noteworthy that all spatial integrals have been performed analytically. This is particularly useful in view of the fact that the Friedel oscillations in $n_0(z)$ lead to oscillatory integrands in surface response calculations.

In Fig. 5 we show results for the image potential

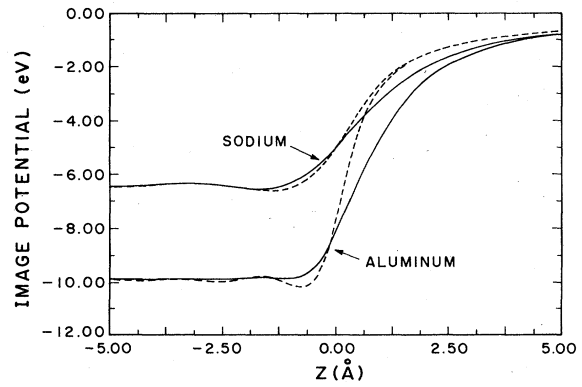

FIG. 5. Image potential $U_{\rm im}(z_1)$ for sodium and aluminum surfaces for a charge $Q_1=e$. The coordinate z_1 is measured from the jellium edge, $z_1<0$ being the metal interior (solid curves). We show by the dashed lines the corresponding results for $U_{\rm im}(z_1)$ in the IBM.

throughout the surface region for both sodium and aluminum surfaces. Here we have set $Q_1=e$. Note that Eq. (3.7) has strict meaning for a quantum-mechanical particle only in the limit of an infinitely heavy mass. It is, however, a reasonable approximation for the case of a heavy impurity placed near the surface, or for an adsorbed atom. Even in the case of an electron the concept of a local image potential has proved useful in surface physics [for example, in the analysis of electron-energy-loss spectroscopy (EELS) experiments[18]].

From Fig. 5 we have that the magnitude of $U_{\rm im}(z_1)$ increases smoothly in the surface region from its asymptotic classical limit ($\sim z_1^{-1}$) at large distance from the surface until it reaches its bulk value for $z_1\sim 2$ Å ($z_1\sim 4$ Å) inside the jellium in the case of aluminum (sodium). The physical reason for the smooth saturation of the image potential at the surface [classically it blows up at the image plane, cf. Eq. (3.8)] is the finite screening length ($\propto k_F^{-1}$) characterizing the electron-gas response in the RPA.

The solid curves shown in Fig. 5 were obtained using the self-consistent electron wave functions $\phi_l(z)$ (obtained by the method of Sec. II) in the computation of $\chi^{(0)}_{mn}(q_{||})$. For purposes of comparison we have also computed $U_{\rm im}(z_1)$ using the IBM in which, we recall, $a_s^{(l)}=\delta_{sl}$ and $z_0=3\pi/8k_F$. The corresponding results are shown by dashes in Fig. 5. It is seen that the main difference between both sets of results occurs outside the jellium. This was to be expected since the IBM electron-density profile is a rather poor approximation to the Lang-Kohn profile for $z_1>0$. For example, for $z_1=1.5$ Å the IBM underestimates $U_{\rm im}(z_1)$ by about 41% in the case of aluminum and by about 25% in the case of sodium. Note that this value of z_1 is representative of atom or molecule-surface distances in chemisorption [e.g., for CO chemisorbed on Cu (100)]. Our results thus indicate that the use of the IBM in such a case[19] is not quantitatively reliable.

Now the total energy of interaction between the external charge (assumed in what follows to be a proton) and the surface is given by

$$U_{\rm tot}(z_1)=U_{\rm im}(z_1)+U_{\rm el}(z_1)\ , \tag{3.9}$$

where $U_{\rm el}(z_1)$ is the energy of the electrostatic interaction with the dipolar layer at the "bare" surface, given by

$$U_{\rm el}(z_1)=-V_H(z_1)\ , \tag{3.10}$$

$V_H(z_1)$ being given by Eq. (2.7). Note that while $U_{\rm im}(z_1)$ corresponds to an attractive interaction for charges of either sign, $U_{\rm el}(z_1)$ corresponds to a repulsion for the present case in which the external charge is positive and to an attraction for a negative charge. Note also that $U_{\rm el}(z_1)$ vanishes identically for a classical model of the surface [in which $n_0(z)$ coincides with the jellium profile (2.8)].

In Fig. 6 we show $U_{\rm tot}(z_1)$ for an aluminum surface as a function of the distance between the proton and the surface, measured from the jellium edge. As a consequence of the competition between attractive ($U_{\rm im}$) and repulsive ($U_{\rm el}$) interactions, $U_{\rm tot}(z_1)$ develops a potential well with a minimum at $z_1\cong 0.36$ Å and a depth of 5.15 eV measured from the vacuum level.

A similar linear-response calculation of $U_{\rm tot}(z_1)$ was performed some years ago by Ying *et al.*[4] in their density functional theory of chemisorption. However, whereas Ying *et al.*[4] used an extended Thomas-Fermi treatment of the kinetic-energy functional, the RPA response function used in the present work places no restrictive assumptions on the kinetic energy of the electrons. The other difference between the work of Ref. 4 and the present one is that the former includes local exchange and correlation effects, and these are absent in the RPA. Now the equilibrium position of the proton obtained by Ying *et al.*[4] is $z_1 \cong 0.57$ Å, which happens to be in good quantitative agreement with the value obtained in more elaborate, nonlinear-response calculations.[20,21] The interesting question then arises of whether the difference between the values $z_1 = 0.36$ and 0.57 Å for the proton equilibrium site is due to exchange-correlation effects or to kinetic-energy effects, or both. We have recently included[22] local exchange and correlation in the kernel of Eq. (3.2), and have recomputed $U_{\rm tot}(z_1)$. We find that the new equilibrium site is shifted further away from the result obtained in the nonlinear theories (we obtain $z_1 \cong 0.31$). This is so because the effect of exchange and correlation is to make the attractive part of the well shown in Fig. 6 (the image potential) somewhat deeper. Thus, as asserted by Gunnarsson *et al.*,[20] the approximations of linearity and gradient expansion of the kinetic energy must give the "correct" value of the proton equilibrium site by cancellation of errors.

Now a quantity of interest in, for example, the analysis of large-angle, high-resolution EELS,[18] and in physisorption studies, is the location of the effective image plane, $z_{\rm im}$. It is known[3,4] that $z_{\rm im}$ gives the position of the center of mass of the charge induced at the surface by a point charge placed infinitely far from the surface. In our theory the value of $z_{\rm im}$ can be extracted directly from Eq. (3.7). For $z_1 \gg d$ the exponential in Eq. (B1) acts as an effective cutoff. Thus in this limit we rewrite Eq. (3.7) as

$$U_{\rm im}(z_1) = -\frac{e^2}{2}\int_0^\infty dq_{||} e^{-2q_{||}(z_2-d)}(a + bq_{||} + \cdots) \tag{3.11}$$

$$= -\frac{e^2}{4x_1}\left[a + \frac{b}{2x_1} + \cdots\right], \tag{3.12}$$

where we have made the definition

$$x_1 = z_1 - d\ . \tag{3.13}$$

From our numerical solution for $\chi_{mn}(q_{||})$ for $q_{||} \to 0$ we have [using Eqs. (3.7) and (B1)] that $a = 1$ to six significant figures; this serves as a check of our numerical procedure. Comparing Eq. (3.12) with a similar expansion of the classical result (3.8) in inverse powers of x_1, we conclude that

$$x_{\rm im} \equiv z_{\rm im} - d = \frac{b}{2}\ . \tag{3.14}$$

In Table I we give the results obtained for $z_{\rm im}$ via the numerical evaluation of the coefficient b for aluminum and sodium surfaces. These results, obtained carrying out an 11-layer—film calculation, remain unchanged when the computation is performed for thicker films. Thus, the values of $z_{\rm im}$ given in Table I represent the semi-infinite medium results.

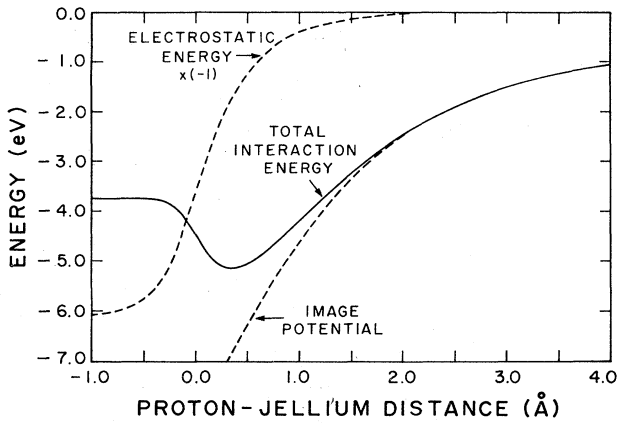

FIG. 6. Total proton-surface interaction energy $U_{\rm tot}(z_1)$, for an aluminum substrate. Also shown are the attractive (image potential) and repulsive (dipole barrier) contributions to $U_{\rm tot}(z_1)$.

In Table I we first give $z_{\rm im}$ (measured from the jellium edge) obtained using the wave functions $\phi_l(z)$ associated with the Lang-Kohn profile obtained as described in Sec. II (full RPA results). We also give the results obtained using the IBM. The comparison of both sets of calculations highlights the inadequacy of the IBM: Whereas for the correct $n_0(z)$ the center of mass of the induced charge lies in the tail of the electron-density profile, in the IBM it lies inside the jellium. This feature of the IBM is shared by the even coarser approximation known as the semiclassical IBM,[17] in which $n_0(z)$ exactly replicates the jellium background. (In that case $z_{\rm im}$ lies even deeper into the jellium.)

For purposes of comparison, in Table I we quote the results obtained by Lang and Kohn[3] for $r_s = 2.0$ and 4.0 (for aluminum and sodium the corresponding values of r_s are 2.07 and 3.93). The difference between the results of Lang and Kohn and the RPA results obtained in this work (note that their results place the image plane farther out in the tail) must be attributed to the presence of (local) exchange and correlation effects in the response calculation of Ref. 3. This conclusion, supported by very recent results of Rasolt and Perrot[23] within the IBM, has been

TABLE I. Position of the effective image plane $z_{\rm im}$, measured from the jellium edge. We compare the results of the full RPA calculation performed using the self-consistent electron wave functions $\phi_l(z)$ with those obtained using the IBM for these wave functions. Also shown are the density functional results of Lang and Kohn.

	Aluminum $z_{\rm im}$ (Å)	Sodium $z_{\rm im}$ (Å)
RPA	0.65	0.32
IBM	−0.32	−0.36
Lang-Kohn	0.85	0.69

verified explicitly by including local exchange and correlation in the kernel of Eq. (3.2).[22] It would be of interest to include *nonlocal* exchange and correlation effects in the computation of $z_{\rm im}$. (This may yield a smaller value for $z_{\rm im}$.)

B. Total energy of interaction between two charges placed near a metal surface

When two charges Q_1 and Q_2 are placed at positions $\vec{R}_1$ and $\vec{R}_2$ in the vicinity of a metal surface, in addition to the direct (free-space) Coulomb interaction between them there is an indirect interaction mediated by the polarization of the surface: The screening charge induced by the presence of one of the charges interacts with the second charge (and vice versa).

Now, the subject of lateral interactions between charges, e.g., adsorbed atoms and molecules, near a metal surface has received a great deal of attention in recent years.[5,24–30] Various models of different degrees of sophistication have been used in treating the substrate surface response[5,26,27] and the quantum-mechanical nature of the adsorbed species.[28,29] Furthermore, experimental evidence of the importance of the electronic mechanism for lateral interactions between adsorbed atoms has been given.[30] Here our objective is twofold. First, as was done above in the evaluation of the image potential, we wish to illustrate the usefulness of the method introduced in Sec. II. Second, we believe a calculation of the energy of the lateral interaction of two (classical) charges in which the surface response is obtained by the full solution to a well-defined microscopic model, such as the RPA, to be of considerable interest in itself.

The indirect energy of interaction $W^{(i)}(\vec{R}_1;\vec{R}_2)$ equals the potential energy of the charge at $\vec{R}_2$ due to its interaction with the charge density induced at the surface by the charge at $\vec{R}_1$ (or vice versa). Thus

$$W^{(i)}(\vec{R}_1;\vec{R}_2)=\int d^3x \int d^3x' U_{\rm ext}(\vec{x};\vec{R}_1)\chi(\vec{x};\vec{x}') \times U_{\rm ext}(\vec{x}';\vec{R}_2)\ , \tag{3.15}$$

where $U_{\rm ext}(\vec{x};\vec{R}_{1,2})$ is defined by Eq. (3.5). Alternatively, Eq. (3.15) may be viewed as giving the work done in bringing the charge Q_2 from infinity to $\vec{R}_2$ against the field of the charge density $-en_{\rm ind}(\vec{x})$ induced at the surface by the charge at $\vec{R}_1$ (classically, by the *fixed* image of Q_1).

By introducing the two-dimensional Fourier transforms of $\chi(\vec{x},\vec{x}')$ and of the Coulomb potential, and the representation (3.4) for $\chi(\vec{q}_{||}\,|\,zz')$, the integrals in Eq. (3.15) are performed analytically. We are thus led to the result that

$$W^{(i)}(\vec{R}_1;\vec{R}_2)=W^{(i)}(R_{||};z_1,z_2) \tag{3.16}$$

$$=\int_0^\infty dq_{||}\,J_0(q_{||}R_{||})\sum_{mn}B_{mn}(q_{||}\,|\,z_1,z_2) \times\chi_{mn}(q_{||})\ , \tag{3.17}$$

where $R_{||}$ is the distance between the two charges in the x-y plane,

$$R_{||}=|\,\vec{R}_{1||}-\vec{R}_{2||}\,|\ , \tag{3.18}$$

and $J_0(x)$ is the Bessel function of order 0. The matrix $B_{mn}(q_{||}\,|\,z_1,z_2)$ is given in Appendix C.

Figure 7 shows the result of computing $W^{(i)}$ for an aluminum surface. We have set $Q_1=Q_2=e$ and $z_1=z_2=z$, i.e., we placed both charges (e.g., protons) on the same plane parallel to the surface, at a distance z from the jellium edge. The four solid curves are labeled by the corresponding value of z. We note that the curve for $z=-1$ Å is indistinguishable, on the scale of the figure, from the results obtained for values of z deeper inside the medium.

Now, the results shown in Fig. 7 appear to be in conflict with the result of Lau and Kohn[5] regarding the existence of a long-range *oscillatory* indirect interaction between two charges placed near a metal surface. However the result of Lau and Kohn (derived for noninteracting electrons) refers only to the contribution to $W^{(i)}(\vec{R}_1;\vec{R}_2)$ from a very weak singularity in the integrand for $q_{||}=2k_F$. More precisely, the fourth derivative of the integrand of Lau and Kohn's expression for $W^{(i)}(\vec{R}_1;\vec{R}_2)$ has a square-root singularity for $q_{||}\to 2k_F$ from above. From this result they obtain the following asymptotic behavior:

$$W^{(i)}(R_{||}\,|\,z,z)\to\mathcal{F}(z)\frac{\cos(2k_FR_{||})}{R_{||}^5}\ , \tag{3.19}$$

for large values of $R_{||}$ and for z in the vicinity of the jellium edge, where $\mathcal{F}(z)$ is a function of z.

It is then of interest to display the contribution to Eq. (3.17) from the interval $2k_F\le q_{||}\le\infty$. This is done in Fig. 8. The oscillatory contribution to $W^{(i)}$ is indeed present. Furthermore, the period of the oscillations is π/k_F, which immediately implies the existence of a singu-

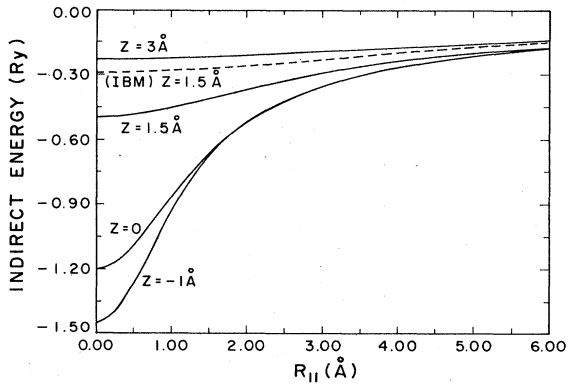

FIG. 7. Indirect energy of interaction $W^{(i)}(R_{||};zz)$ between two protons placed at a distance z from an aluminum surface as a function of their lateral separation $R_{||}$ (z is measured from the jellium edge). We show by the dashed line the IBM result for $z=1.5$ Å.

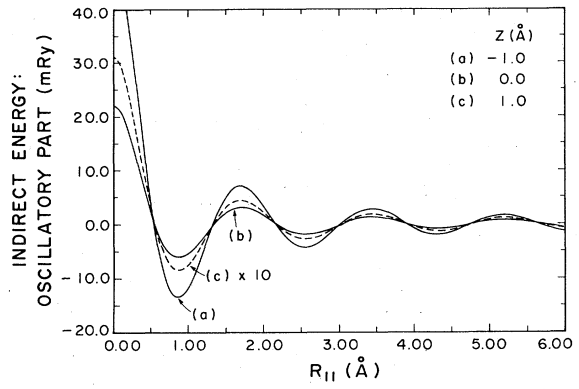

FIG. 8. Oscillatory contribution to the indirect interaction $W^{(i)}(R_{||}\,|\,zz)$ shown in Fig. 7.

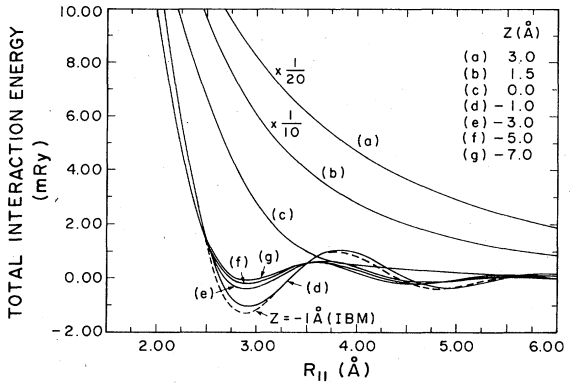

FIG. 9. Total energy of interaction $W^{(t)}(R_{||}\,|\,zz)$ between two protons placed at a distance z from an aluminum surface as a function of their lateral separation $R_{||}$. Note that the period of the oscillations that obtain for negative values of z (i.e., inside the jellium) equals $\pi/k_F = 1.79$ Å.

larity in the integrand of Eq. (3.17) [that is, in $\chi_{mn}(q_{||})$] at $q_{||}=2k_F$. (The singularity is too weak to be apparent in a plot of the integrand.) However, for the range of values of z for which we have computed $W^{(i)}$, the amplitude of the oscillations decays slower than the fifth power predicted by Eq. (3.19) (the decay rate is closer to $R_{||}^{-3}$). Thus the fifth-power decay law must take hold at distances larger than typical adatom-adatom separations. Finally note the rapid decrease in the amplitude of the oscillations as the charges are moved outside the jellium (the curve for $z_1=1.0$ Å has been multiplied by a factor of 10).

The above conclusions are consistent with the approximate analytical results of Johansson[25] concerning the nature of the long-range Friedel oscillations around an adatom. Using the IBM this author finds three distinct regions (if the "adatom" is far from the surface there is a fourth region as well). For $R_{||}<k_F^{-1}$ one has the preasymptotic region. For $R_{||}>k_F^{-1}$ and $R_{||}$ comparable to the adatom-surface distance, an asymptotic expansion is possible, but no simple decay rate of the amplitude of the oscillations in powers of $R_{||}^{-1}$ is found. For even larger values of $R_{||}$ ($R_{||}>10$ a.u. for $r_s=2.07$, according to Fig. 2 of Ref. 25), the decay rate is given by Eq. (3.19). A detailed analysis of the Friedel oscillations in the charge density induced by a surface impurity will be given elsewhere.[22]

We emphasize that the oscillatory indirect interaction depicted in Fig. 8, whose amplitude is of the order of a few millirydbergs, is completely obscured by the much larger, monotonically-decaying interaction (of the order of a rydberg) that arises from the contribution to Eq. (3.17) from the interval $0\le q_{||}\le 2k_F$, which on the scale of the figure is practically the same as the full $W^{(i)}$ shown in Fig. 7. For large values of $R_{||}$ the behavior of the monotonic interaction ($\sim R_{||}^{-1}$) is determined by the behavior of the integrand for $q_{||}\to 0$ (it behaves like $a+bq_{||}$, with $a\neq 0$).

Now, in addition to the indirect interaction given by Eq. (3.17), the two charges interact directly through the free-space Coulomb interaction

$$W^{(d)}(\vec{R}_1;\vec{R}_2)=\frac{Q_1Q_2}{|\vec{R}_1-\vec{R}_2|}\ . \tag{3.20}$$

Note that the two interactions are of opposite sign [for charges of equal sign Eq. (3.17) leads to an attraction and Eq. (3.20) to a repulsion]. Furthermore, they are of the same order of magnitude (fraction of a rydberg). Thus the question arises of whether the *total* energy of interaction

$$W^{(t)}(\vec{R}_1;\vec{R}_2)=W^{(i)}(\vec{R}_1;\vec{R}_2)+W^{(d)}(\vec{R}_1;\vec{R}_2)\ , \tag{3.21}$$

shows a long-range oscillatory behavior by virtue of the large cancellation that obtains upon adding Eqs. (3.17) and (3.20).

Figure 9 shows results for $W^{(t)}(R_{||}\,|\,z,z)$ for an aluminum surface. For completeness, we show in Fig. 10 the corresponding results for a sodium surface. We notice that $W^{(t)}(R_{||};z,z)$ does show long-range oscillations (of period π/k_F) for values of z inside the jellium. However, outside the jellium the oscillations are simply too small in magnitude to be of significance.

A point worth noting in the results given in Figs. 9 and 10 is the relatively slow convergence of the total interac-

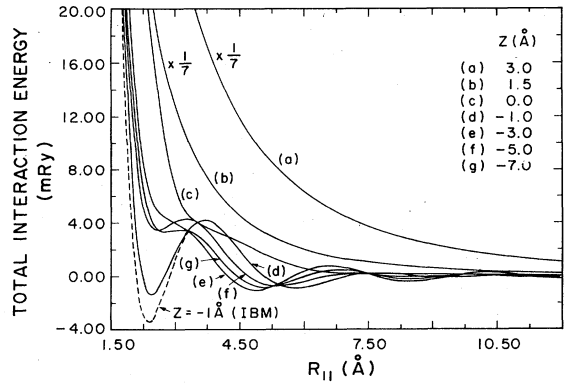

FIG. 10. Same as Fig. 9, but for a sodium surface. The period of the oscillations present for negative values of z equals $\pi/k_F=3.40$ Å.

tion energy as a function of the depth z into the jellium. (In the case of sodium the convergence is oscillatory in nature, cf. Fig. 10.) These results suggest that the effect of the surface on vibrational frequencies near the surface could be rather long ranged.

From our results we conclude that the mechanism considered here (coupling of two charges by the polarization of the electron gas at the surface) does not lead to an overall long-range oscillatory interaction of two charges placed *outside* the jellium ("adatoms") as is the case when the charges are inside the jellium. This conclusion appears to be contrary to current thinking in the field. Of course the coupling mechanism first proposed by Grimley,[26] by which two chemisorbed atoms are coupled by electron tunneling through the substrate, does lead to an oscillatory indirect interaction between the adatoms. This mechanism is outside the scope of the present work.

ACKNOWLEDGMENT

This work was supported by the National Science Foundation Grant No. DMR-82-14214.

APPENDIX A: THE MATRIX $M_{pp'}$

The Hamiltonian matrix $M_{pp'}$ is defined by the equation

$$M_{pp'}=\frac{\hbar^2}{2m}\left[\frac{p\pi}{d}\right]^2\delta_{pp'}+M_{pp'}^{(H)}+M_{pp'}^{(\mathrm{xc})}\ , \tag{A1}$$

where

$$M_{pp'}^{(H)}=\frac{4\pi e^2}{d}\int_0^d dz[n_0(z)-n_+(z)]I_{pp'}(z) \tag{A2}$$

and

$$M_{pp'}^{(\mathrm{xc})}=\frac{2}{d}\int_0^d dz\, V_{\mathrm{xc}}(z)\sin\left[\frac{p\pi}{d}z\right]\sin\left[\frac{p'\pi}{d}z\right]\ . \tag{A3}$$

In Eq. (A2) we have introduced the definition

$$I_{pp'}(z)=\tfrac{1}{2}[I_{pp'}^{(+)}(z)-I_{pp'}^{(-)}(z)]\ , \tag{A4}$$

where

$$I_{pp'}^{(+)}(z)=\frac{d^2}{\pi^2(p+p')^2}\left[1+(-1)^{p+p'}-2\cos\left[(p+p')\frac{\pi}{d}z\right]\right] \tag{A5}$$

and

$$I_{pp'}^{(-)}(z)=\delta_{pp'}\left[z^2-zd+\frac{d^2}{2}\right]+(1-\delta_{pp'})\frac{d^2}{\pi^2(p-p')^2}\left[1+(-1)^{p-p'}-2\cos\left[(p-p')\frac{\pi}{d}z\right]\right]\ . \tag{A6}$$

We note that the integral that defines the matrix $M_{pp'}^{(\mathrm{xc})}$ can only be evaluated numerically. On the other hand, the matrix $M_{pp'}^{(H)}$ can be obtained in closed form. Substituting Eq. (2.9) in Eq. (2.2) and this in Eq. (A2), and carrying out the required (rather lengthy) algebra, we are led to the following explicit alternative result for the matrix $M_{pp'}^{(H)}$:

$$M_{pp'}^{(H)}=\delta_{pp'}\left[\frac{8d}{\pi^2 a_B}U_0-\frac{2\pi z_0\bar{n}_+d^3}{3d}\left[\frac{e^2}{d}\right]\left[1-3\frac{z_0}{d}+2\frac{z_0^2}{d^2}\right]\right]$$
$$-\frac{2d}{\pi^2 a_B}[B_{p,+p'}-(1-\delta_{pp'})B_{p,-p'}]-\frac{4\bar{n}_+d^3}{\pi^2}\left[\frac{e^2}{d}\right]A_{pp'}\ . \tag{A7}$$

In Eq. (A7) we have made the following definitions

$$U_0=\sum_l\Theta(E_F-\epsilon_l)(E_F-E_l)\sum_{s,s'}a_s^{(l)}a_{s'}^{(l)}[1+(-1)^{s-s'}]\left[\frac{\delta_{ss'}}{(4s)^2}-(1-\delta_{ss'})\frac{ss'}{[s^2-(s')^2]^2}\right]\ , \tag{A8}$$

$$B_{p,\pm p'}=\frac{1}{(p\pm p')^2}\sum_l\Theta(E_F-\epsilon_l)(E_F-\epsilon_l)\sum_{ss'}a_s^{(l)}a_{s'}^{(l)}[\delta_{s-s',p\pm p'}+\delta_{s-s',-(p\pm p')}-\delta_{s+s',p\pm p'}-\delta_{s+s',-(p\pm p')}] \tag{A9}$$

and

$$A_{pp'}=[1+(-1)^{p-p'}]\left[\frac{\sin[\pi(p+p')z_0/d]}{(p+p')^3}-(1-\delta_{pp'})\frac{\sin[\pi(p-p')z_0/d]}{(p-p')^3}\right]\ . \tag{A10}$$

Both Eqs. (A2) and (A7) are used in our numerical procedure. We note that in establishing the result given by Eq. (A7) we have used the result

$$\frac{m}{\pi\hbar^2}\sum_l \Theta(E_F-\epsilon_l)(E_F-\epsilon_l)=(d-2z_0)\bar{n}_+ , \quad \text{(A11)}$$

which guarantees the overall charge neutrality of the system.

APPENDIX B: THE MATRIX $A_{mn}(q_{||}\,|\,z_1)$

In this appendix we give the matrix $A_{mn}(q_{||}\,|\,z_1)$ explicitly. This matrix was introduced in the result for the image potential $U_{\rm im}(z_1)$ given by Eq. (3.7). Our result adopts a different form depending on whether the external charge is outside or inside the electron gas. (Recall that in this paper the origin of coordinates has been placed on the left-hand infinite barrier.)

(i) External charge is *outside* the electron gas, $z_1>d$. We have that

$$A_{mn}(q_{||}\,|\,z_1)=\pi e^2Q_1^2e^{-2q_{||}(z_1-d)}q_{||}\frac{[(-1)^m-e^{-q_{||}d}]}{[q_{||}^2+(m\pi/d)^2]}\times\frac{[(-1)^n-e^{-q_{||}d}]}{[q_{||}^2+(n\pi/d)^2]} . \quad \text{(B1)}$$

Note that here z_1-d is the distance between the charge and the right-hand infinite barrier. For $z_1<0$ the definition of $A_{mn}(q_{||}\,|\,z_1)$ is obtained from Eq. (B1) with the replacement $z_1-d\rightarrow|\,z_1\,|$.

(ii) External charge is *inside* the electron gas, $0<z_1<d$. We have that

$$A_{mn}(q_{||}\,|\,z_1)=\frac{\pi e^2Q_1^2q_{||}C_{mn}(q_{||}\,|\,z_1)}{[q_{||}^2+(m\pi/d)^2][q_{||}^2+(n\pi/d)^2]} , \quad \text{(B2)}$$

where we have made the definition

$$\begin{aligned}C_{mn}(q_{||}\,|\,z_1)=&[(-1)^m-e^{-q_{||}d}][(-1)^n-e^{-q_{||}d}]-(1-e^{-2q_{||}(d-z_1)})[(-1)^{m+n}-e^{-2q_{||}z_1}]\\&-4m\left\{\frac{1}{m+n}\left[(-1)^{m+n}-\cos\left[(m+n)\frac{\pi}{d}z_1\right]\right]+\frac{(1-\delta_{mn})}{m-n}\left[(-1)^{m-n}-\cos\left[(m-n)\frac{\pi}{d}z_1\right]\right]\right\}\\&+4\left[(-1)^m[e^{-q_{||}d}+(-1)^n]-\cos\left[\frac{m\pi}{d}z_1\right]\right][(-1)^ne^{-q_{||}(d-z_1)}+e^{-q_{||}z_1}] . \quad \text{(B3)}\end{aligned}$$

APPENDIX C: THE MATRIX $B_{mn}(q_{||}\,|\,z_1,z_2)$

The matrix $B_{mn}(q_{||}\,|\,z_1,z_2)$, introduced in Eq. (3.17), takes a different form depending on whether both charges are outside the electron gas, inside it, or one is inside while the other is outside. For brevity we now give the results for the first two cases only. (These are the cases considered in Sec. III.)

(a) Both charges are *outside* the electron gas, $z_1>d$ and $z_2>d$. We have that

$$B_{mn}(q_{||}\,|\,z_1,z_2)=2\pi e^2Q_1Q_2e^{-q_{||}(z_1+z_2-2d)}q_{||}\times\frac{[(-1)^m-e^{-q_{||}d}]}{[q_{||}^2+(m\pi/d)^2]}\times\frac{[(-1)^n-e^{-q_{||}d}]}{[q_{||}^2+(n\pi/d)^2]} . \quad \text{(C1)}$$

(b) Both charges are *inside* the electron gas, $0<z_1<d$ and $0<z_2<d$. We have that

$$B_{mn}(q_{||}\,|\,z_1,z_2)=2\pi e^2Q_1Q_2q_{||}\frac{a_m(z_1)}{[q_{||}^2+(m\pi/d)^2]}\times\frac{a_n(z_2)}{[q_{||}^2+(n\pi/d)^2]} , \quad \text{(C2)}$$

where we have made the definition

$$a_m(z_1)=2\cos\left[\frac{m\pi}{d}z_1\right]-[e^{-q_{||}z_1}+(-1)^me^{-q_{||}(d-z_1)}] . \quad \text{(C3)}$$

[1] J. F. Dobson and G. H. Harris, Phys. Rev. B **27**, 6542 (1983).
[2] W. Kohn and L. J. Sham, Phys. Rev. **140**, A1133 (1965).
[3] N. Lang and W. Kohn, Phys. Rev. B **7**, 3541 (1973).
[4] S. C. Ying, J. R. Smith, and W. Kohn, Phys. Rev. B **11**, 1483 (1975).
[5] K. W. Lau and W. Kohn, Surf. Sci. **75**, 691 (1978).
[6] N. D. Lang and W. Kohn, Phys. Rev. B **1**, 4555 (1970).
[7] G. P. Alldredge and L. Kleinman, Phys. Rev. B **10**, 559 (1974).
[8] D. A. Campbell, A. A. Maradudin, and R. F. Wallis, Solid State Commun. **45**, 125 (1983).
[9] G. P. Kerker, Phys. Rev. B **23**, 3082 (1981).
[10] K. M. Ho, J. Ihm, and J. D. Joannopoulos, Phys. Rev. B **25**, 4260 (1982).
[11] P. J. Feibelman, J. A. Appelbaum, and D. R. Hamann, Phys.

Rev. B **20**, 1433 (1979).
[12]J. Bardeen, Phys. Rev. **49**, 653 (1936).
[13]D. M. Newns, Phys. Rev. B **1**, 3304 (1970).
[14]A. Griffin and J. Harris, Can. J. Phys. **54**, 1396 (1976).
[15]A. G. Eguiluz, Phys. Rev. Lett. **51**, 1907 (1983). See also Ref. 22.
[16]D. E. Beck and V. Celli, Phys. Rev. B **2**, 2955 (1970); G. Korzeniewski, T. Maniv, and H. Metiu, J. Chem. Phys. **76**, 1564 (1982).
[17]P. J. Feibelman, Prog. Surf. Sci. **12**, 287 (1982).
[18]B. M. Hall, S. Y. Tong, and D. L. Mills, Phys. Rev. Lett. **50**, 1277 (1983).
[19]B. N. J. Persson and M. Persson, Surf. Sci. **97**, 609 (1980).
[20]O. Gunnarsson, H. Hjelmberg, and B. I. Lundqvist, Phys. Rev. Lett. **37**, 292 (1976).
[21]N. D. Lang and A. R. Williams, Phys. Rev. B **18**, 616 (1978).
[22]A. G. Eguiluz (unpublished).
[23]M. Rasolt and F. Perrot, Phys. Rev. B **28**, 6749 (1983).
[24]F. Flores, N. H. March, and I. D. Moore, Surf. Sci. **69**, 133 (1977).
[25]P. Johansson, Solid State Commun. **31**, 591 (1979); P. Johansson and H. Hjelmberg, Surf. Sci. **80**, 171 (1979).
[26]T. B. Grimley, Proc. Phys. Soc. London **90**, 751 (1969).
[27]T. L. Einstein and J. R. Schrieffer, Phys. Rev. B **7**, 3629 (1973).
[28]J. P. Muscat, Surf. Sci. **110**, 85 (1981).
[29]B. N. J. Persson, Surf. Sci. **116**, 585 (1982).
[30]C. Nyberg and C. G. Tengstal, Phys. Rev. Lett. **50**, 1680 (1983).